INSTITUTE OF PHYSICS PUBLISHING NANOTECHNOLOGY
Nanotechnology **15** (2004) 1135–1151 PII: S0957-4484(04)79431-3

Feature-oriented scanning methodology for probe microscopy and nanotechnology

Rostislav V Lapshin

Solid Nanotechnology Laboratory, Institute of Physical Problems, Zelenograd, Moscow, 124460, Russia

E-mail: lapshin@niifp.ru

Received 13 April 2004
Published 1 July 2004
Online at stacks.iop.org/Nano/15/1135
doi:10.1088/0957-4484/15/9/006

Abstract
A real-time scanning algorithm is suggested which uses features of the surface as reference points at relative movements. Generally defined hill- or pit-like topography elements are taken as the features. The operation of the algorithm is based upon local recognition of the features and their connection to each other. The permissible class of surfaces includes ordered, partially ordered, or disordered surfaces if their features have comparable extents in the scan plane. The method allows one to exclude the negative influence of thermodrift, creep, and hysteresis over the performance of a scanning probe microscope. Owing to the possibility of carrying out an unlimited number of averages, the precision of measurements can be considerably increased. The distinctive feature of the method is its ability of topography reconstruction when the ultimate details are smaller than those detectable by a conventional microscope scan. The suggested approach eliminates the restrictions on scan size. Nonlinearity, nonorthogonality, cross coupling of manipulators as well as the Abbé offset error are corrected with the use of scan-space-distributed calibration coefficients which are determined automatically in the course of measuring a standard surface by the given method. The ways of precise probe positioning by local surface features within the fine manipulator field and the coarse manipulator field, automatic probe return into the operational zone after sample dismounting, automatic determination of exact relative position of the probes in multiprobe instruments, as well as automatic successive application of the whole set of probes to the same object on the surface are proposed. The possibility of performing accurately localized low-noise spectroscopy is demonstrated. The developed methodology is applicable for any scanning probe devices.

1. Introduction

With a scanning probe microscope (SPM), there are some restrictions on the ultimate precision of measuring surface elements. The restrictions are caused by noises inherent in the instrument. One of the widespread ways to reduce noise is multiple averaging of the obtained data. Since a scanning probe microscope is subjected to thermodrift [1–5] and creep [6, 7], the efficiency of averaging declines dramatically and practically becomes zero.

In order to help suppress the above fundamental distortion factors, an active scanning and positioning method [8, 9] is suggested whose main idea consists of using features of the surface under investigation as reference points at movements. The movements are performed from one feature to another one located in the vicinity. As a result, a connected sequence (chain) is formed, where the features are placed relatively to each other. The search, detection and calculation of feature position coordinates are all made by a real-time recognition program [9, 10]. By scanning a small domain (segment) around each feature followed by laying out the obtained fragments by the proper positions within the found chain, the actual surface topography can be reconstructed. The effect is achieved due to the localization, relative nature and multiple iterations

of measurements, ceaseless probe attachments to surface features [11, 12] as well as the use of counter displacements hierarchy.

The permissible class of surfaces includes all surfaces with atomic relief, surfaces consisting of molecules, all kinds of chains, clusters, grains, particles, crystallites, quantum dots, pillars, pores, 2D-patterns, 2D-textures and so on; i.e., all that generally falls under the definition of a hill or a pit. The above surfaces may be ordered, partially ordered, or disordered as well. The main restriction imposed on the class of surfaces is as follows: the lengths of the objects must be comparable in different directions of the scan plane so as to have the feature completely localized in a segment. Unsuitable surfaces, for instance, are a defectless surface of a 1D diffraction grating, a surface of integrated circuit with a great number of long conducting wires, and so forth.

2. Description of the methodology

2.1. Algorithm of the feature-oriented scanning: operation principles and main procedures

The principle of the scanning algorithm is founded on the notions of locality and connection; the objects that the algorithm operates with are surface features, and the method itself may be called object- or feature-oriented scanning (FOS). In fact, the method implements a transition from absolute coordinates of a scanner to relative ones associated with surface features.

It should be noted that, as a rule, the features are the subject of research or technology, and in addition the given method proves to be ineffective when scanning surfaces with a small number of features or surfaces where features are completely absent. Strictly speaking, there are no absolutely smooth surfaces; the question is usually just whether the features on the particular surface meet the measurement scale that the researcher is currently engaged in as well as if the features are contrasted and stable enough to serve as reliable reference places.

With the method suggested, the surface scan is obtained in two stages. First, a 'seed' is built, which is a quasi-straight chain of features (feature line or FL) with fixed length oriented in a given direction. The seed serves as an initial setting element. Second, the rest of the scan is developed from the formed seed by using local connection. There are two ways of local connection that may be used herein.

The first way (see figure 1) implies a round over the seed with joining up the new chain elements. While scanning, the probe moves exclusively by the nodes of the growing chain. It is much like tracklayer work: it always runs along the railroad which it builds itself. Once the 'next' chain feature is found, it is labelled as the 'current' one, added to the chain and becomes part of the round contour.

The second method (see figure 2) implies that the probe moves by lines of features which serve as auxiliaries. The first FL is the seed; all the others are formed dynamically during the scan process. The chain body consists of elements of the first FL and features selected from the neighbourhoods of features of the current FL while moving the probe from the last feature of the latter to its first one. It is like a tracklayer run along

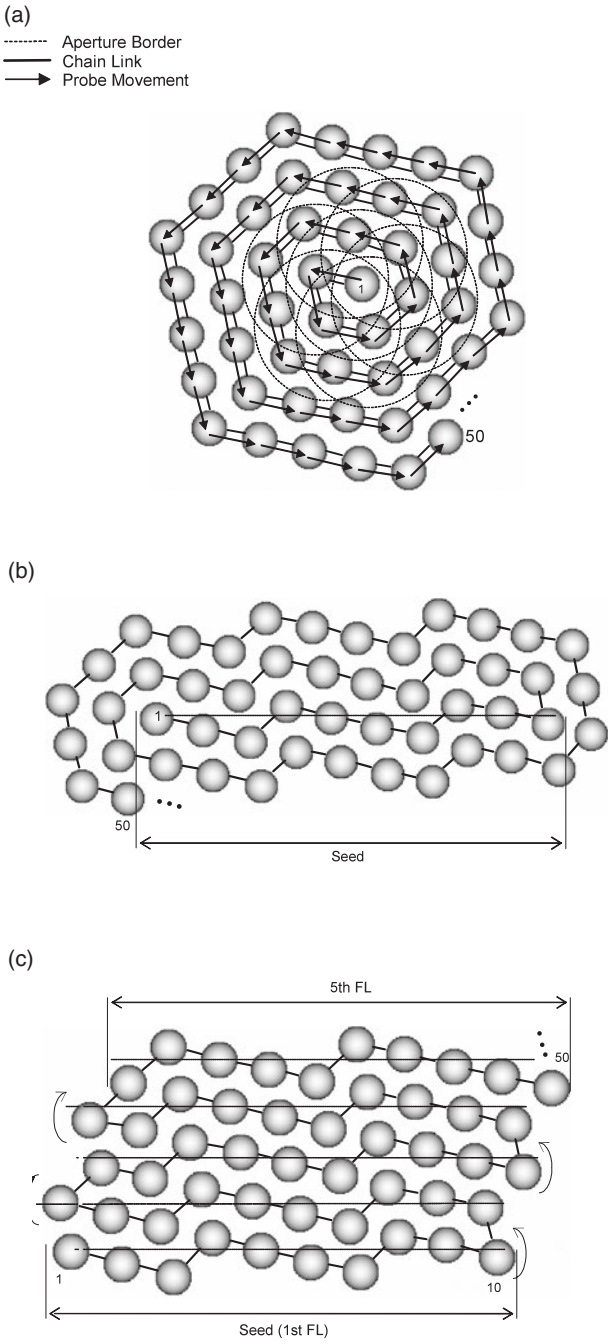

Figure 1. The stylized images of carbon atoms of a graphite surface illustrate the simplest ways of local connection by means of a seed round with joining. The seed: (a) a single atom; (b), (c) quasistraight chain of 10 atoms. The direction for round over a contour: (a), (b) fixed (counterclockwise); (c) alternate (switching at the end of each FL).

an existing railroad creating a new one in parallel. Having achieved the first feature in the current FL the probe switches to the last feature of the next FL.

Thus, with the scanning method, the trajectory of probe movement is not predefined; only the system behaviour pattern is preset in advance in a general form so as to select the next chain feature.

After the first chain feature is specified and labelled as 'current', the probe attachment procedure is deblocked.

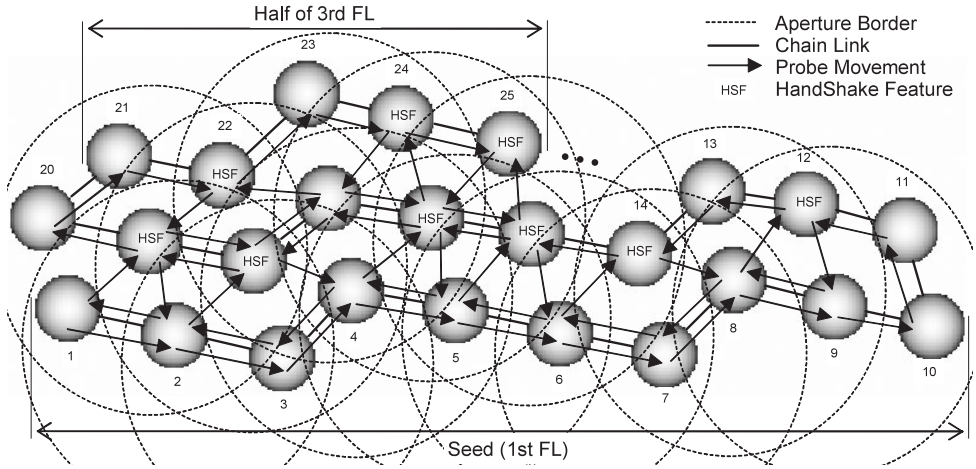

Figure 2. Local connection of features by using auxiliary FLs. The first FL is a seed. The handshaking atom is intended for the connection of adjacent groups of atom-neighbours belonging to adjacent atoms of the current FL.

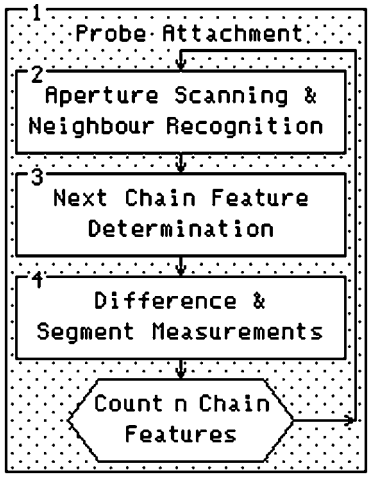

Figure 3. Simplified flowchart of the FOS algorithm. The probe attachment procedure works in the background. The scan is considered done when the chain length reaches a set value n.

From that moment on the procedures described below will be executed step by step (see figure 3).

2.1.1. Procedure of probe attachment to surface feature. The procedure of probe attachment carries out a line scan of a segment, namely, a square neighbourhood of the current chain feature (see figure 4(a)). After that, the procedure recognizes the current feature (i.e., the one nearest to the raster centre), calculates its absolute coordinates, then moves the probe to the found position of the current feature, and then the above operations are repeated in a certain time interval T.

Thus, the attachment procedure ensures holding the microscope probe above the surface feature chosen during practically unlimited time. It removes the feature image displacement within the sight of view of the device as a consequence of the microscope's lateral drift. In fact, the procedure represents a software lateral plane digital follow-up system. Moreover, the algorithm adjusts automatically to changes in drift value, considering its time fluctuations.

2.1.2. Procedure of scanning the aperture and recognition of the nearest neighbours. First, the procedure implements a common line scan of the surface within a square window. The size of the window is set so as to cover, with some margins, the nearest neighbours of the current feature (see figure 4(b)). Further surface analysis is carried out within either the actual scan window or a circle inscribed in it, both being called hereafter an aperture.

Then, the procedure recognizes features and finds among them the current feature, i.e., the one nearest to the raster centre. The coordinates of the neighbour features are determined relative to the absolute current feature position. Actually, the given procedure also performs the probe attachment, yet less accurately since the aperture size is a few times greater than the segment size.

2.1.3. Local connection: procedure of determination of the next chain feature. This procedure runs in different ways depending on the scanning stage or the method used for local connection. It should be noted that the principal and most appreciable shortcoming of the method of composing a surface scan by rounding over a seed followed by joining is its inability to correctly select among the feature neighbours those which do not belong to the chain already passed out after the chain has reached a certain length. The reason for that consists of the error being accumulated as the chain grows. The value of the error must not exceed a half of the typical distance between features.

With virtual scanning (i.e., with FOS simulation on conventionally obtained images) that error is insignificant but with physical (real) scanning it can become apparent rather quickly. Here, the larger the noises and changes in drift velocity are, the faster the pointed restriction occurs, some set number of averages being applied. That, in its turn, puts a limit to the maximum scan size for the given microscope.

To illustrate the above, figure 5 presents a stylized image of a graphite surface; the measurement is carried out in the real mode. Distortions are easily noticeable in the picture: the change in step of the spiral and the concavity increase as the chain grows.

As an alternative, the method of connection using auxiliary FLs (see figure 2) can be suggested to avoid misconnections provoked by accumulated errors in the chain. Its main idea

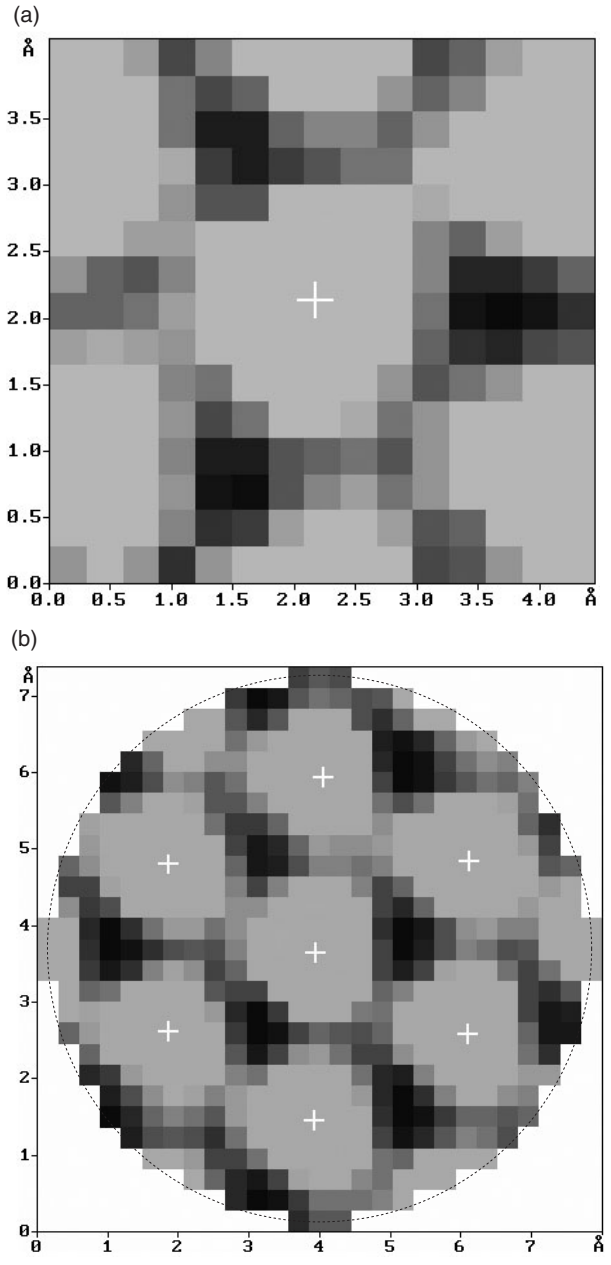

Figure 4. A typical view of (a) a segment and (b) an aperture of the ordered graphite surface after recognition. Steps of the microscope in the lateral plane: $\Delta x = 0.296$ Å, $\Delta y = 0.273$ Å. The atom positions found are marked with a '+' sign. The atom nearest to the raster centre is the one considered as 'current'. The segment side is 15 pixels. The aperture side is 27 pixels.

is to make as few chain elements as possible potentially take part in the neighbour sorting operation, i.e., the chain should be inspected at the least possible depth.

To do that, a group of neighbours of the current feature of the current FL is formed which includes the only features not belonging to the FL and lying at the same predetermined side of it. In fact, here we deal with a round again but this time the current feature of the current FL is rounded, i.e., it is an essentially small, non-growing structure. Connection of adjacent groups of feature-neighbours related to adjacent features of the current FL is carried out using a 'handshaking' feature, i.e., the current feature of the growing chain.

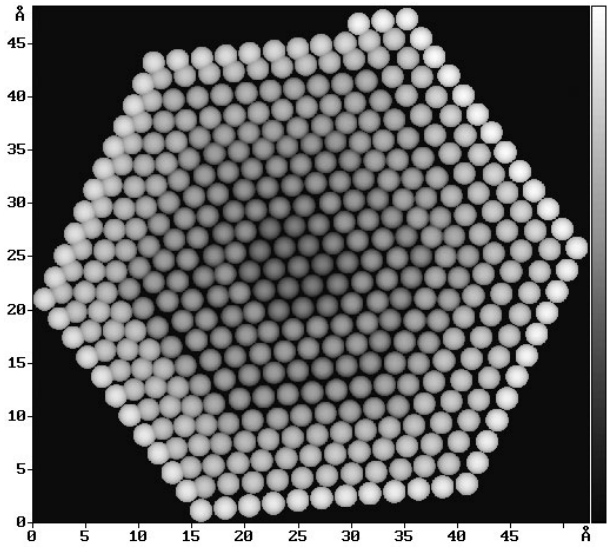

Figure 5. Typical real-scan distortions: change in spiral step and nonexistent concavity of the image caused by the effect of error accumulation in the chain. The chain length n is 400 carbon atoms.

In order to suppress the error accumulation in a chain, a correction should be made periodically when adding new chain links. This implies 'dissolution' of the discrepancy along the chain section from the current atom to one of the obtained neighbours inserted in the chain at the previous coil/FL. Note in conclusion that in case no features suitable to serve as the next have been found among the neighbours during the connection process, the aperture radius is enlarged and the scan and analysis of the aperture are run again.

2.1.4. Skipping: the procedure of measuring the differences and the segments. This procedure measures precisely the coordinates of the next chain feature relatively to the current one. At the beginning, the microscope probe is moved to the next feature position where a conventional line scan is carried out of its square neighbourhood-segment. Later on, recognition is carried out and the absolute coordinates of the next feature are determined. Then, the procedure calculates the 'forward' (current-to-next) coordinate differences, and moves the probe backwards to the current feature position and does there the same as has just been done to the next feature. As the absolute coordinates of the current feature are found, the procedure calculates the 'backward' (next-to-current) coordinate differences between the features.

The above sequence referred to hereafter as skipping is repeated as many times as the number of averagings is specified (there are no principal limitations to the number of averagings). Finally, the next feature gets tagged as the current one, and the counter of chain features is incremented by a unit. Remember that the relative coordinates for the first probe movement to the position of the next feature are determined by the procedure of aperture scanning and recognition.

Provided the change in drift velocity is rather small (see section 3.6) during a skipping cycle (∼300 ms for atom relief surfaces), the drift is compensated quite completely. Let, for example, x projection of drift coincide with x projection of the probe movement from the current to the next feature. In

that case the measured difference is greater than the actual one. While moving the probe in the reverse direction the difference obtained is less than actual by the same magnitude. Therefore, the mean value of these differences is equal to the true distance between the features (drift elimination in the counter-scanned segments is described in [13]).

As surfaces with features larger than atomic are scanned, creep begins to strongly dominate over thermodrift. However, the resulting effect from the creep self-generation does not appear to be great, since in the present method, surface topography is measured by parts, i.e., small segments located close by, and all probe transitions occur only between neighbouring features at short distances. Another reason for this is a vast application of mutually-opposite displacements in the apertures, in the segments, at the skipping, and at the movement along FLs. It should be underlined that in the method suggested, some displacements have no opposite components. In order to reduce the creep produced by such displacements, an after movement pause of a necessary duration can be automatically introduced as a sequence of probe attachment cycles.

Though the contrary displacements do not compensate for creep completely, yet the drift generated by them would change slowly overall and therefore can be eliminated using the linear scheme pointed above (see section 3.7). Applying FOS one should bear in mind that the bigger the features used, and the more distant they are from each other, the larger the measurement error is.

In this connection, joint use of both hills and pits is preferable, certainly if both are available on the surface. Although on a single-processor computer the recognition time increases, it remains constant on a two-processor computer as the task of recognition can be easily run in parallel: one processor is busy with the hills and the other one with the pits on the same image. Since the smallest and the most densely packed features are atoms and internodes on crystalline solid surfaces, those surfaces should be considered the most suitable for the FOS method suggested.

Besides accurate determination of the relative coordinates of the next feature in a chain, the skipping procedure does the averagings of surface segments, which permits one to effectively suppress noise and to reach high resolution in the vertical plane. It is necessary to note that the segment size must be chosen so as the segments of the neighbour features partially overlap each other ensuring surface 'assemblage' with no gaps (see section 2.3).

Since the relative distance between the features obtained during skipping is a real number that is changing by a probability law, by doing a great number of measurements of the differences and the segments and increasing the number of pixels and the height levels of the real surface at assemblage, it is possible to reconstruct the topography with overall lateral and vertical details more finely (the tip is supposed to be sharp) than those the microscope is capable of revealing with usual scanning (see section 3.2).

Note in conclusion that in the described FOS algorithm

(1) A segment is an area of the utmost localization of topography measurements.
(2) No more than two features exist at the same time with known absolute coordinates (two features at the skipping and one in all other states). Coordinates of the rest of the chain features are relative.
(3) The obtained chains are intrinsically free of piezomanipulator hysteresis-related errors as all the movements with FOS are performed exactly from one feature to another.
(4) The proposed algorithm is deadlock-free and, what is most important, the results of its operation do not depend on a unit cell type or on its sizes; they are also insensitive to defects or feature disorder on the surface. Here, objects too large to fit in the segment are bypassed and objects too small to be reproduced from scan to scan are ignored.
(5) FOS termination may occur not only on the chain having grown up to the stated number of features but also on having completely filled up a rectangular scanning window with the topography of the surface under investigation (see section 2.4). That window is set up by the microscopist beforehand so that, from the outside, the FOS looks like conventional scanning.
(6) The FOS algorithm can be considered among adaptive ones since it includes units providing self-adjustment to the current environmental conditions, surface features, and the particular equipment.

2.2. Distributed calibration of microscope scanner

The distributed calibration consists of scanning a standard surface such as, for example, highly oriented pyrolytic graphite (HOPG) by the suggested algorithm and determining local calibration coefficients by skipping between a chain feature and all its nearest neighbours. As a result, instead of three fixed calibration coefficients [10], a distribution pattern (net) of calibration coefficients in the scanning space is obtained. Since the influence of thermodrift and creep is eliminated during the measurement, the calibration net turns out to be independent of velocity and direction of scanning (see section 3.7). Thus, using distributed calibration data it is possible to eliminate in one procedure all spatial distortions caused by nonlinearity, nonorthogonality, and cross coupling of piezomanipulators while assembling a surface (see the next section) [9].

Invariability of the standard surface structure in each point of the scanner field is of great importance when seeking the distributed coefficients. However, that is not always feasible in practice because of defects, though this is not an insurmountable obstacle. If the microscope is equipped with a coarse XY manipulator, a preliminarily chosen 'perfect' part of the crystal surface can be moved within the fine manipulator field using the procedure of probe attachment to the feature (see section 2.5.2). Thus, it is possible to calibrate the whole scanner field from a small area of the standard.

2.3. Scan data visualization: surface assembler and stylizer

The following procedures are to be used for the purpose of viewing the image obtained: surface assembler, which reconstructs a real surface out of the segments, and stylizer, which creates a hypothetical surface where the atoms are imaged schematically by balls [8–10].

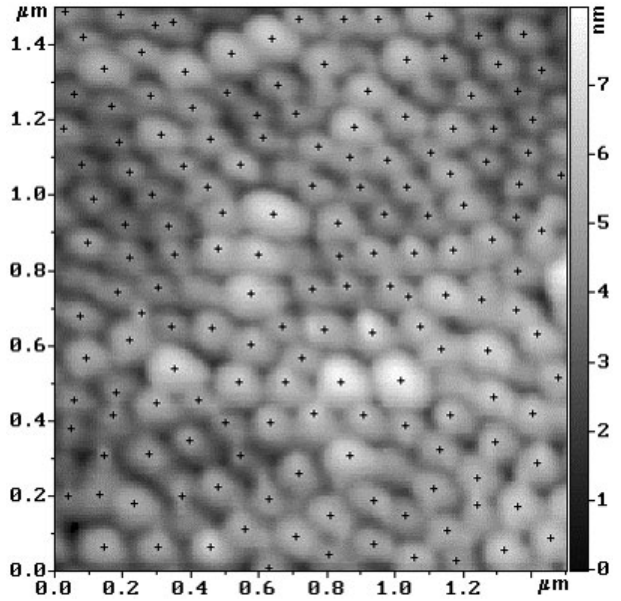

Figure 6. Reconstruction of a disordered nanostructured aluminium surface. Local connection: a seed round with joining. '+' sign designates positions of the chain features (hills). Fixed-size segment: (45×45) pixels^2 (1 pixel is equal to approximately 72 Å). The mean size of the aperture side is 69 pixels. The number of aperture adjustments is 52.

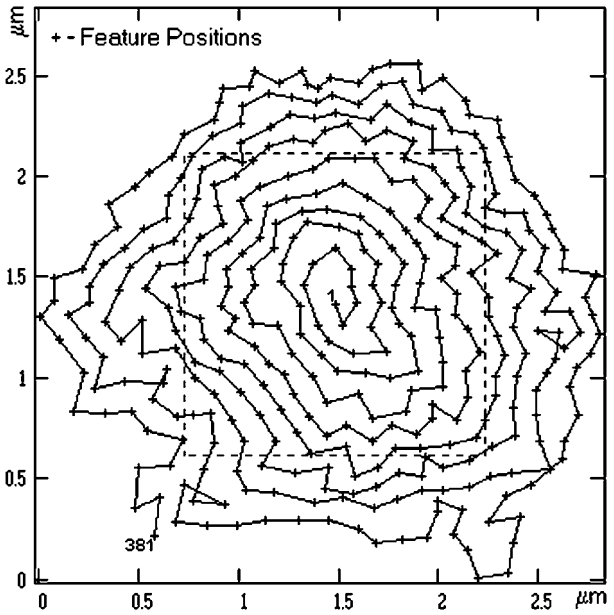

Figure 7. 'Web'—trajectory of 'probe movement' from one feature to another during the chain formation. The borders of the window being filled up are shown with a dotted line.

The surface assembler searches the whole chain for features with lateral coordinates lying within the visualization window set by the microscopist. When the next feature is found, the assembler puts its segment to the corresponding position of the image being built. While assembling, first, drift is corrected within the counter-scanned segment [13], then, the segment position and positions of each point within the segment are corrected by using the interpolated calibration coefficients calculated by the net values nearest to the positions being corrected. Finally, at those locations where the adjacent feature segments overlap each other, the topography is averaged out. Note that any image scanned in the common way may be corrected by using distributed calibration data.

2.4. Specifics of disordered surface scanning

Properties typical of scanning a disordered surface are: direct recognition of surface features (search and screening of topography generalized saddle points are used) [9], transition from a fixed segment size to a variable one, as well as change of scanning step (scale) in case the aperture has reached its size limit and no suitable candidate for the next chain feature is found among the neighbours.

Figure 6 presents the result of virtual scanning of a disordered nanostructured aluminium surface that has been prepared by electrochemical polishing of textured aluminium foil [14]. Termination of the virtual scanning occurred after filling up a preset (1.5×1.5) μm^2 window; the applied connection method was a seed round with joining. The initial image was obtained with an atomic force microscope (AFM) in tapping mode. The reconstructed image shown in figure 6 and the initial image are both identical. Since the size dispersion of the features (aluminium pillars) in the lateral plane did not prove to be large, a fixed size segment was used at the scanning. In figure 7, it is shown how separate features are connected in the obtained chain (compare with figure 1(a)). A segment and aperture typical of the disordered surface are presented in figure 8.

Figure 9 illustrates the feature connection in the same area of the disordered aluminium surface by means of auxiliary FLs. Jagged edges of the image presented indicate that it consists of separate segments. Figure 10 reflects the connections in the obtained chain and the chain structure, namely, the orientation, length, total quantity, and switching positions of the FLs. However, the actual trajectory that the 'probe moved' from one feature to another ensuring correct connection looks much more complicated (see figure 11, in comparison with figure 2).

With scanning an ordered surface, the main sign to consider when selecting features suitable for probe attachment is the square of the feature basement. In the real mode the threshold value is set up with some reserve to ensure selection reliability. When scanning a disordered surface, for any set threshold there may always be found features with basement square values near that threshold.

In the virtual mode that would not lead to any 'fatal' consequences. In the real mode it is just the opposite: there exists a probability that a feature with such a 'floating' square value detected in the aperture may be omitted in the segment because of noises and instabilities (the omission of such a feature in the aperture is not critical for connection). To avoid that, while recognizing the neighbours of the current feature in the aperture, the threshold must be increased by the value of the occurring uncertainty.

The further growth of detection reliability is provided by introducing some additional signs, the simplest of which being feature height. In case both hills and pits are used as features simultaneously, an additional sign would be the concurrence of feature types—hill or pit. The feature volume, and the structure

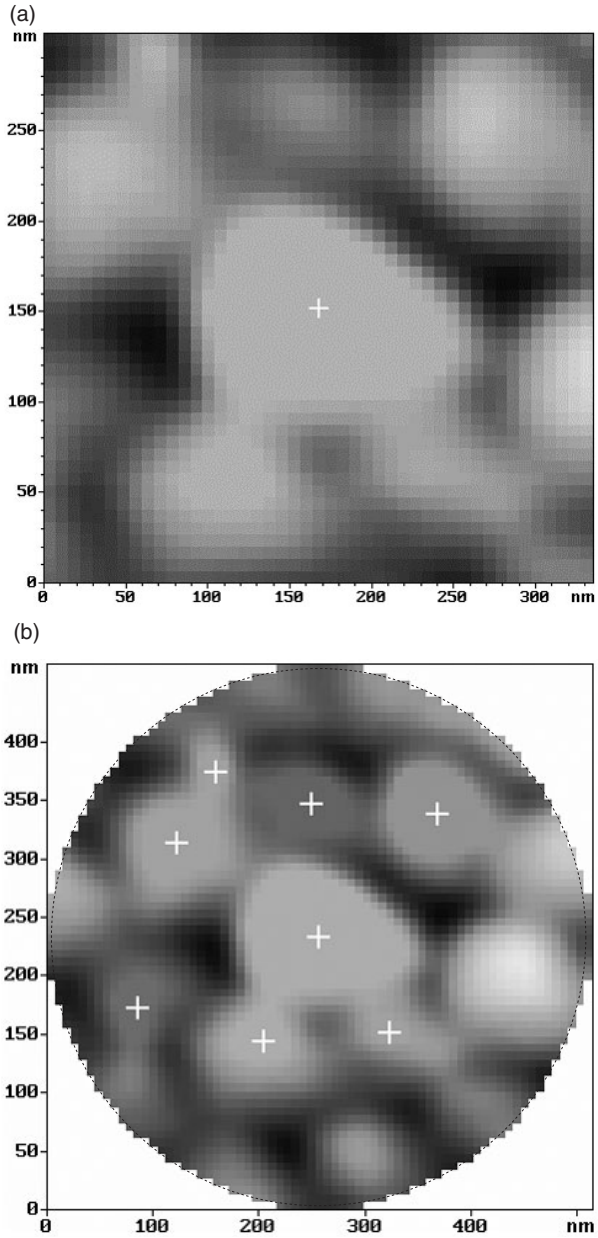

Figure 8. A typical view of (a) a segment and (b) an aperture of the disordered aluminium surface after recognition. The feature nearest to the raster centre is the current one.

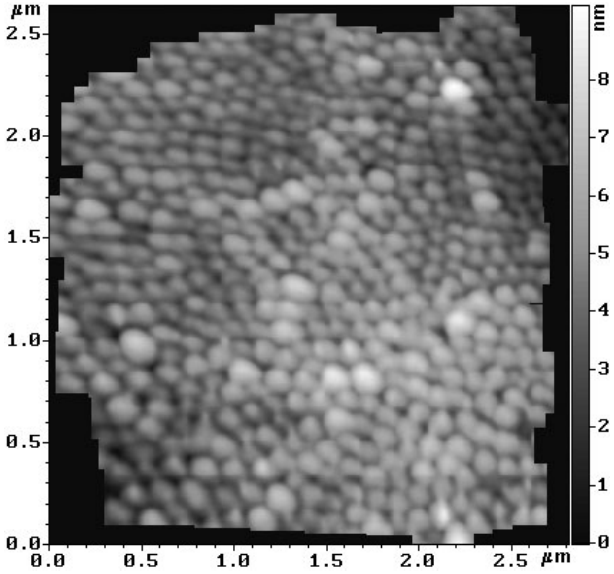

Figure 9. Reconstruction of disordered aluminium surface. Connection is carried out by using auxiliary FLs. Fixed-size segment: (45×45) pixels^2. The mean size of the aperture side is 73 pixels. The number of aperture adjustments is 57.

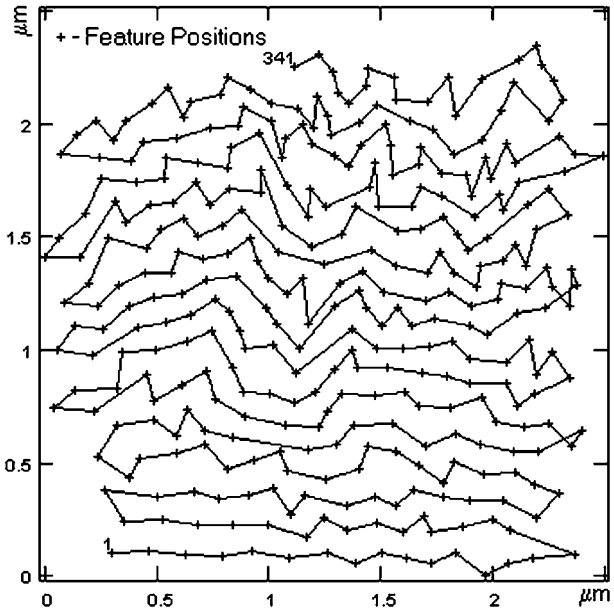

Figure 10. Chain structure or 'skeleton' of the disordered aluminium surface. Easily distinguishable are the sequence of feature connection, length and orientation of FLs, and switching positions of FLs.

of the nearest neighbours can serve as identifying signs; also feasible are methods even more complicated in regard to computational technique which are based on correlation analysis, searching for signs characterizing the feature contour form, etc. Provided that in the course of surface topography measurement under high vacuum conditions spectroscopic data, which carry information of local surface chemical compound or local surface mechanical properties, are also obtained, those data may also be used as feature distinguishers at recognition.

2.5. Technique of positioning by local surface features

2.5.1. Probe movement within the field of a fine manipulator. Router. Depending on the experimental or technological task to be solved, the microscope probe positioning is carried out in one of the two following methods. The first method actually represents the seed formation process, i.e., among the neighbours such a feature is searched for which is located at the lowest angle to the movement (seed) direction. When the probe movement occurs by atoms exactly along a crystallographic direction, the position of the next chain atom found may be used to adjust the motion direction constantly (see section 3.4), which allows one to follow precisely along the chosen crystallographic direction independently of its possible curvature or the presence of point lattice defects.

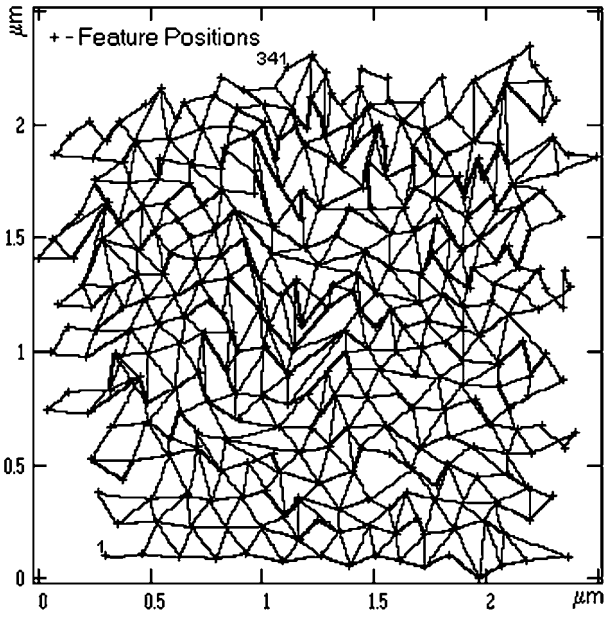

Figure 11. 'Net'—trajectory of 'probe movements' at connection. Some movements are invisible because of the overlap of lines.

The second method implies a preliminary FOS of the surface; therefore it essentially requires much time for positioning. In order to make a move, a special procedure called 'router' extracts a subchain out of the whole chain such that it connects the current probe position with the desired terminal one by any trajectory determined by the experimentalist thus laying a route. Then, scanning the aperture and recognizing the nearest neighbours at each path step, the router moves the probe to the position best corresponding to the chosen route data. The process is repeated until the probe reaches the terminal feature of the trajectory.

If a more accurate positioning within the vicinity of the terminal feature is still required, the positioning is done by moving the probe relative to the feature location. The time span while the probe is permitted to be aside from the feature corresponds to the interval T between successive attachments.

2.5.2. Probe movement within the field of a coarse manipulator. With existing SPMs, a coarse XY manipulator provides the starting position for a fine manipulator within its whole field which is the surface area available for investigation after the sample has been mounted. The coarse manipulator travels with a rather big step usually not exceeding the fine manipulator work range. The direction, value, speed, and displacement step of the coarse positioner are set manually by the operator.

It is impossible to move precisely from one point of the accessibility field on the sample surface to any other point outside the current fine scanner range mostly because of the irregularity of the coarse positioner step as well as hysteresis, thermodrift, creep, and cross talking. Hand-operated settings also introduce some uncertainty. Thus, with most of the currently available instruments, the relative position of the scans yielded by a fine manipulator in different parts of the coarse manipulator field cannot be defined accurately, and therefore the whole image cannot be built correctly.

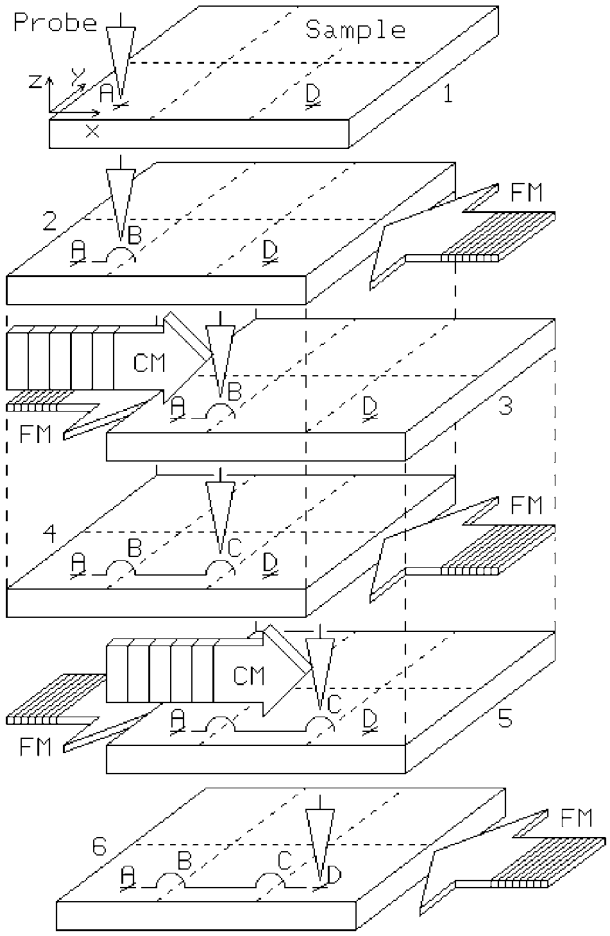

Figure 12. Accurate travel of the microscope probe from point A to point D at a distance more than one range of the fine manipulator. Designations: FM is the fine manipulator, CM is the coarse manipulator. Dotted lines on the sample show the coarse manipulator field partitioning into adjacent ranges of the fine manipulator. The arcs in the probe positions B and C symbolize some surface features.

To be unambiguous, let us assume the sample under investigation to be mounted on the fine manipulator, and the probe on the coarse one. For the sake of simplicity, a one-dimensional case will be considered (see figure 12); the probe is to be moved from point A to point D.

Initially, the microscope probe is located at the surface point A (pos. 1). Let the fine manipulator move the probe relative to the surface towards point D until the range boundary is reached (see pos. 2, point B). If positioning is carried out in the usual way then the feature nearest to point B is being searched for and captured. Otherwise, if positioning is carried out by features then the current chain feature is used instead. After that, the coarse manipulator makes a step towards point D (pos. 3). At the same time the attachment procedure is running cyclically, aiming to compensate for the arising displacement by means of the fine manipulator.

Further on, the coarse manipulator followed by the fine one keeps on moving until the fine manipulator range is used up. Thus, as the positioners are travelling jointly, it restores to the fine manipulator the possibility of moving the probe further to the right relative to the surface. Then, the above operations

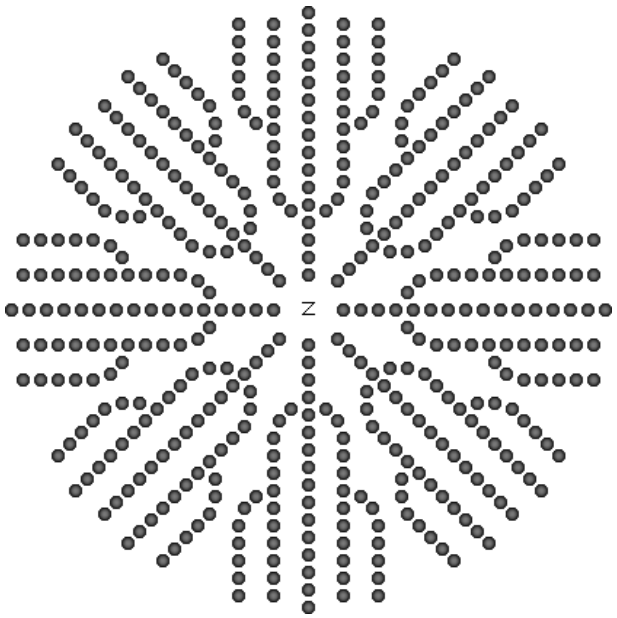

Figure 13. Snowflake-like navigation structure as a system of feature chains converging into an operational zone (designated as *z*).

are repeated (see pos. 4, 5) making the probe move to the right across the surface as far as one range of the fine manipulator and reach the point C. Finally, the probe moves to the desired point D drawn by the fine manipulator (pos. 6).

Movement errors and nonlinearities are more or less typical of any type of coarse manipulator. Usually their absolute values exceed the corresponding parameters of fine manipulators by orders. A distinctive feature of the suggested method [9, 15] is that the errors and nonlinearities of the coarse manipulator do not affect the allocation of the fine manipulator field within the coarse one. It is shown by analysis that the 'walking' type of positioners [16] best meets the requirements of the described method.

2.5.3. Automatic probe return into an operational zone. Let us consider one of the useful applications of the feature-oriented positioning algorithm: automatic return of the microscope probe into the operational zone [8, 9]. This function is required in SPM experiments where after the surface has been subjected to some kind of local probe action (mechanical indentation, scratching, oxidation, heating, electrical field evaporation, and so on), the sample is dismounted, exposed to a non-local treatment (film growing, etching, annealing, and so on), and mounted back again so as to watch the surface changes at the place affected.

To realize automatic movement to the point of modification, a ramified system of feature chains must be created on the initial sample surface which converges to the operational zone. In figure 13, an example of such a structure is presented. Now, it will suffice to catch any structure feature immediately after the probe approach, then to set up (approximately) an appropriate direction of movement towards the zone and to wait until the probe reaches the terminal chain element autonomously.

As the above is extended, an artificially manufactured substrate surface structure can be suggested to connect several technological zones to each other. Provided a feature size hierarchy exists in the structure, a more precise and quicker positioning can be realized. The latter is especially important when separate atoms or molecules are used as technology objects. Supplementing the described approach by the ability of carrying out accurate probe movements on a large coarse manipulator field (see previous section), a quite reliable way is obtained to transfer the nanolithograph end effector.

2.5.4. Automatic determination of the positional relationship between the probes in multiprobe instruments. With a real nanotechnology process, it is reasonable to apply an SPM lithograph equipped with probes of two types: analytical and technological ones. Analytical probes are intended for measurements and for check-ups while technological probes are used for surface modifications. The discrimination is necessary because the probe tip usually undergoes modifications in the course of a nanolithography process such as changes in radius, form, and physicochemical properties. Each of those types may be further specialized, e.g., one analytical probe serves as topography measurement tool and another for spectroscopy; one technological probe is used for local influence by electric field while another for indentation, etc.

The suggested feature-oriented technique provides for connecting the probes, i.e., accurately determining their mutual location as well as applying all kinds of probes to the same objects thus implementing a sequence of various technological operations with different tools. Automatic probe connection is also necessary in highly productive multiprobe microscopes for correctly assembling the whole image out of fragments obtained simultaneously while surface scanning with a probe array.

Suppose it is required to connect an analytical probe to a technological probe. By scanning with those two probes a certain surface area located within the reach of both probes, surface images are obtained and then subjected to recognition. After that, it is possible to determine (roughly) the shift value in the coordinate systems of the probes by revealing a surface feature on the image scanned with the technological probe and detecting the same feature on the image scanned with the analytical probe. Finally, in order to increase the precision of the measurement by eliminating the influence of drift and noise, a set number of skipping cycles of the probes should be carried out (here, instead of one probe and a pair of features we have one feature and a pair of probes).

The probes can be connected in a chain by moving from one probe to another probe adjacent to the first one, each time using a new feature within the overlap area of their scan fields. Otherwise, the probes can also be connected using the same feature by 'passing' that feature over from one pair of adjacent probes to another pair by means of the coarse positioner followed by ceaselessly repeated probe attachment (see section 2.5.2). Besides connection, the last trick provides for consecutively applying any number of analytical and technological probes to any surface feature and any point of that feature neighbourhood.

3. Experimental results

One of the problems that arose when practically realizing the real mode of the FOS concerned instabilities while scanning

an aperture or a segment. The algorithm suggested is capable of automatically revealing most of the instabilities and eliminating their influence by rescanning. If instability occurs during the skipping, the current cycle is declared idle, and the results of its measurements are rejected. Rescanning is repeated in cycles until the change in drift velocity becomes less than a previously set value.

When conducting long-run experiments and/or moving a probe across a sample surface at long distances, the fine Z manipulator may be exceeded. The cause of that is a drift of the microscope head and/or a tilt of the sample surface. With the positioning method proposed, when the fine Z manipulator approaches the edge of its range, the 'pause' state is automatically initiated, and commands which alternate with attachments of the microscope probe to the current surface feature are sent to the coarse Z manipulator in order to return the fine Z manipulator to the middle of its range.

All the measurements were performed in the ambient environment on a scanning probe microscope Solver^{TM} P4 (NT-MDT Co.) placed on a heavy base with passive vibrational isolation provided. The microscope was covered with a passive thermoisolating box for better thermostabilization. The instrument was controlled by a 100 MHz computer. While scanning, no correction for the error accumulated in the chain was carried out. While assembling real surfaces, no corrections were made for drift-produced segment distortions, nonlinearity, obliquity or coupling of manipulators.

3.1. Feature-oriented scanning of atomic relief on a graphite surface

Figure 14 shows a scanning tunnelling microscope (STM) image of an atomic HOPG surface obtained with the algorithm suggested. A mechanically cut NiCr wire was used as the tip. Local connection of the features is carried out by using auxiliary FLs. The positions of some atoms in the scan (see the stylized image) are noticeably distorted because of large temporal instabilities and the small number of averagings of the chain links. The averaged lattice constant differs from its nominal value 2.464 Å, which means that the microscope is decalibrated. Artefacts connected with the segment structure of the image (a) are practically invisible. The low noise level in the segment image should be pointed out despite no kind of data smoothing being performed.

3.2. High resolution feature-oriented scanning of atomic relief on a graphite surface

A small area on a graphite surface was scanned in the high resolution mode (see figure 15). During the experiment, 1000 segments and coordinate differences were obtained for each of the seven carbon atoms. Feature connection was carried out by rounding-and-joining a contour. The seed type is a single atom. After topography assemblage, the lateral and the vertical resolution of the microscope was improved 20 times. In the top left and bottom right corners the initial sizes of the image element corresponding to the minimum step of the microscope can easily be seen (compare also with figure 4(b)).

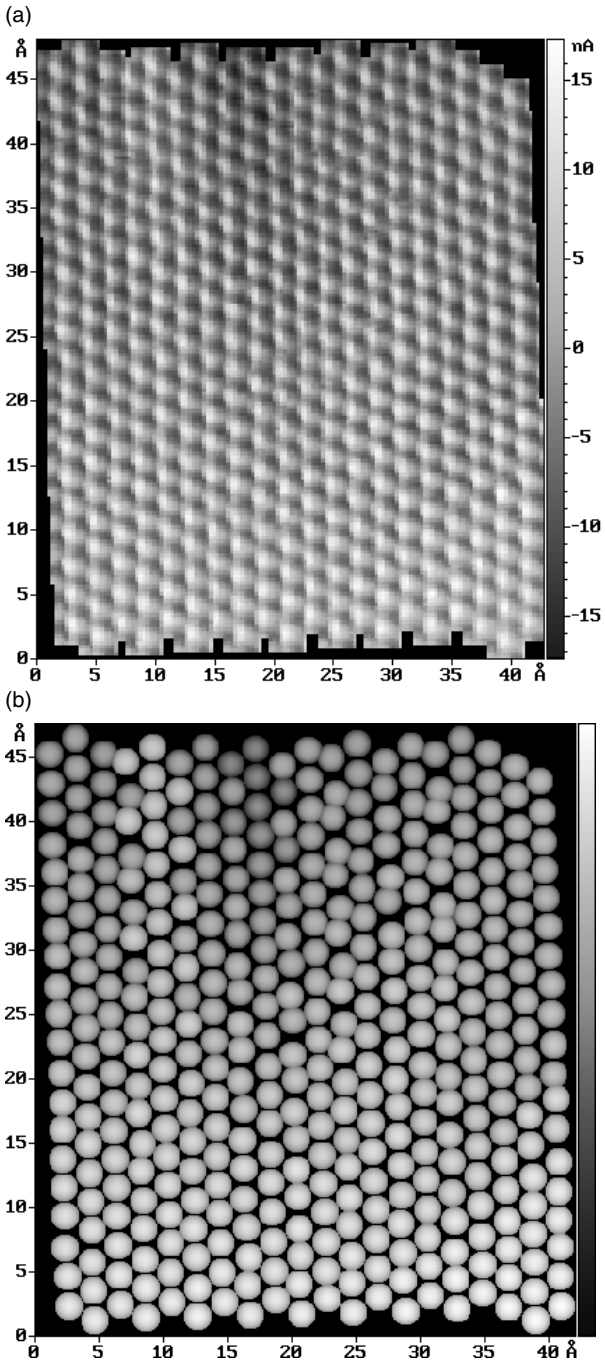

Figure 14. Atomic HOPG surface. (a) Real surface reconstructed from segments (STM, constant Z mode, $U_{\text{tun}} = -10$ mV, $I_{\text{tun}} = 998$ pA). (b) Stylized image or ball model of the surface. The chain length is 400 atoms. The number of samples per raster point is 2. The number of skipping cycles is 3. The number of segment averagings is 6. The mean crystalline lattice $a = b = 2.299$ Å. Mean compactness is 71%. The scanning velocity in the aperture is 1637 Å s^{-1}. The scanning velocity in the segment is 860 Å s^{-1}. The movement speed at skipping is 2.4 μm s^{-1}. The mean modulus of the lateral drift velocity is some 0.51 Å s^{-1}. The measurement time is 23 min.

3.3. High precision measurements of graphite lattice constants and crystallographic directions

Actually, measurement of the lattice constant is a skipping with a great number of averagings ($10^3 \cdots 10^6$). Since the

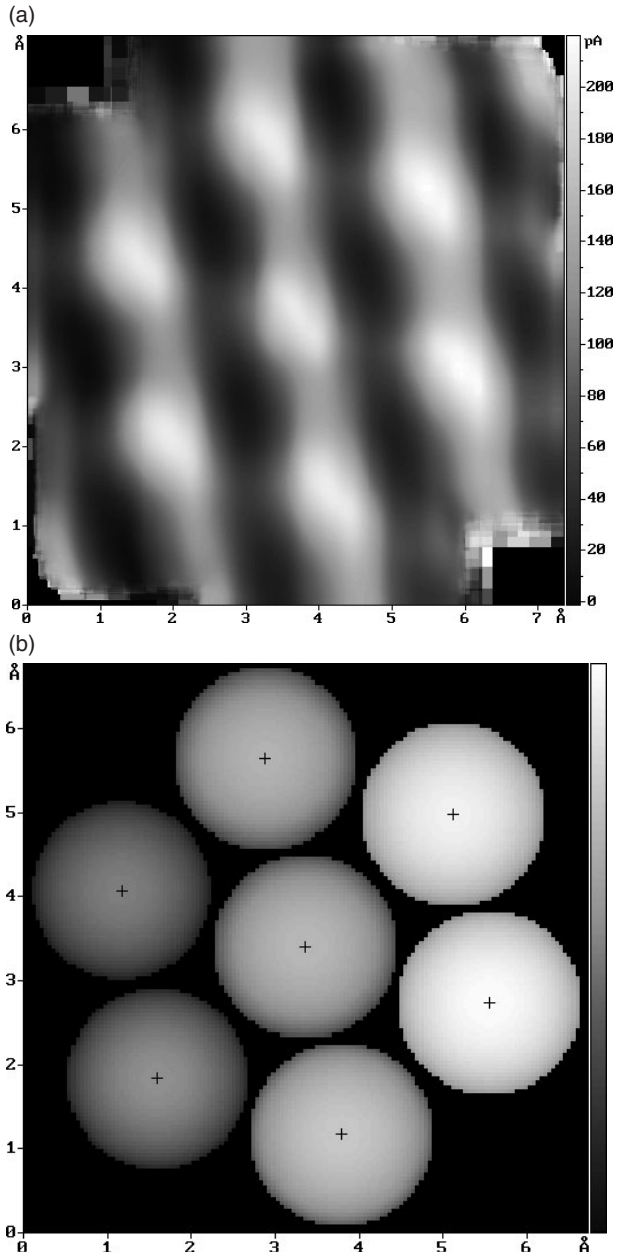

Figure 15. Atomic HOPG surface obtained in the high resolution mode. (a) Raw segmented image (STM, constant Z mode, $U_{\text{tun}} = 15$ mV, $I_{\text{tun}} = 401$ pA). (b) Stylized image. The number of samples per raster point is 3. The number of segment averagings is 1000. The mean crystalline lattice $a = b = 2.299$ Å. The scanning velocity in the aperture is 1285 Å s^{-1}. The scanning velocity in the segment is 665 Å s^{-1}. The movement speed at skipping is 61 Å s^{-1}. The mean modulus of the lateral drift velocity is some 0.19 Å s^{-1}. The scanning time is 39 min.

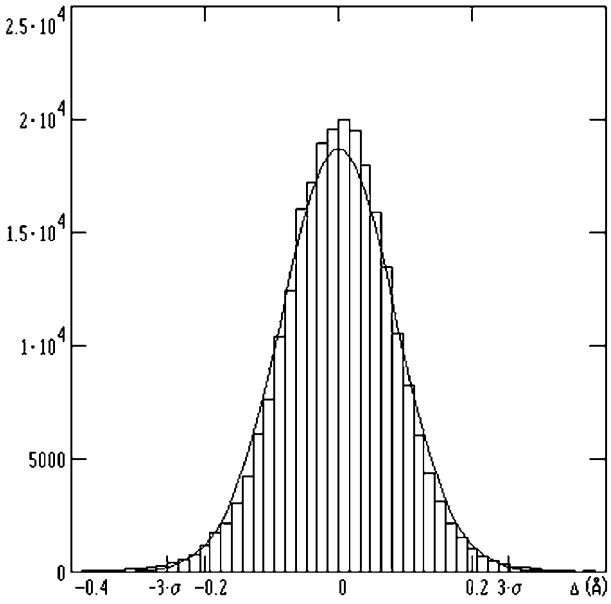

Figure 16. Error distribution histogram for measurement of the HOPG lattice constant. The number of measurements is 2.5×10^5. The one-shot measurement error (3σ) is ± 0.255 Å. Skewness $k_{\text{s}} = -0.09$. Kurtosis $k_{\text{k}} = 1.27$. The measurement time is 7.5 h.

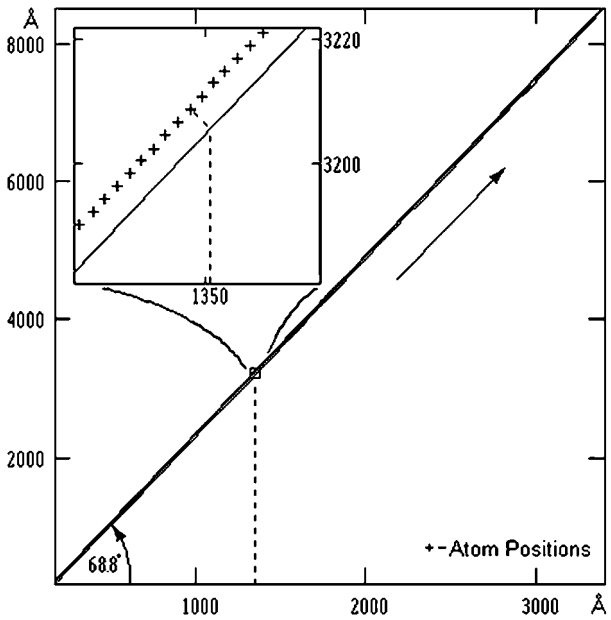

Figure 17. Movement of STM probe by carbon atoms in the set direction on the HOPG surface. The direction constraint submode is activated. The traversed path length $L \approx 1$ μm. The number of atoms in the chain is 4060. The number of skipping cycles is 3. The movement velocity is 1 atom s^{-1}.

orientation of a segment connecting two features is measured during the skipping relative to the X manipulator axis, in the general case to determine the angle between crystallographic directions on the surface, a skipping of another feature pair is required followed by computation of the difference in the obtained orientations.

250 000 measurements of the HOPG lattice constant were carried out in the experiment. It took 7.5 h of ceaseless STM functioning to have the work completed. As a result, the lattice of graphite has been determined with an error of $\pm 0.000\,51$ Å (a one-shot measurement error gives ± 0.255 Å with probability of 0.9973). The distribution function of the measurement error Δ of the crystalline graphite lattice is shown in figure 16. A normal distribution function is also presented to compare it with.

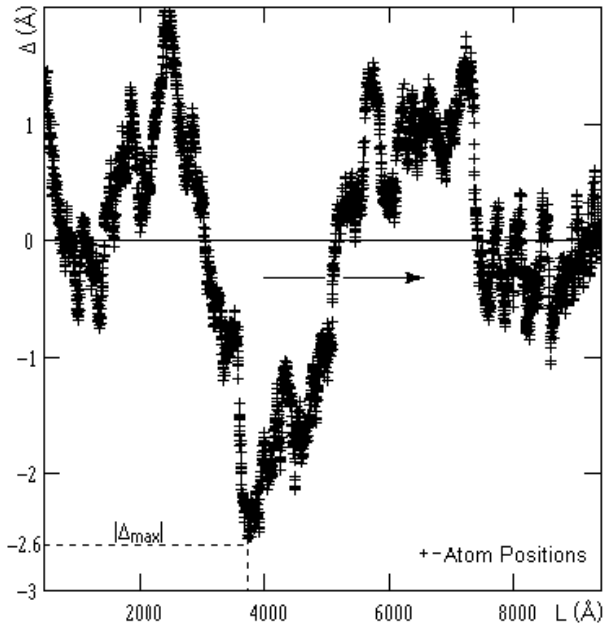

Figure 18. Δ deviations of the chain atom positions from the averaging straight line. The cross-chain nonlinearity is 0.03%.

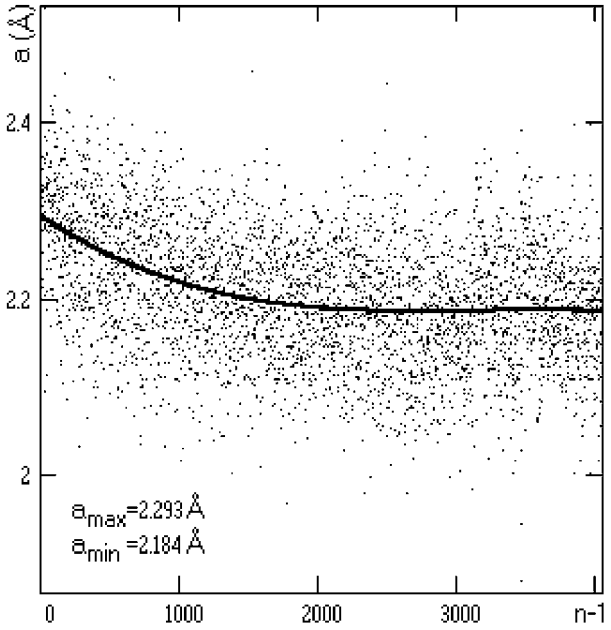

Figure 19. The change of the atomic period a while advancing along the chain. Mean value $\bar{a} = 2.205$ Å. The regression was carried out using a cubic polynomial. The along-chain nonlinearity is 4.94%.

3.4. Operative positioning on atomic graphite surface. Estimation of nonlinear distortions

An STM tip movement (see figure 17) was carried out on an HOPG surface along a crystallographic direction in order to confirm experimentally the possibility of precise positioning on an atomically smooth surface [8, 9, 17] as well as to demonstrate the ability of accurately measuring distances of some microns by counting atomic periods. The traversed path length L made up $\sim$1 μm (chain length: 4060 carbon atoms, movement velocity: 1 atom s^{-1}).

Supposing that the intrinsic distortion of the graphite lattice is insignificant in the mesoscopic scale, the nonlinearity of the microscope scanner can be estimated by the data acquired. With the use of a least mean squares method, an averaging straight line is drawn through the measured positions of the atoms (see figure 17). This line is admitted as a kind of reference structure when determining nonlinearity. The greatest cross-deviation from linearity $|\Delta_{\max}|$ (see figure 18) was some 2.6 Å or $|\Delta_{\max}|/L100\% = 0.03\%$.

Any slight chain curvature being neglected, the along-chain nonlinearity may be defined by the change in the atomic period (see figure 19) as $(a_{\max} - a_{\min})/\bar{a}100\%$, where $a_{\max}$, $a_{\min}$, $\bar{a}$ are maximal, minimal, and mean chain periods, respectively. A large scattering of neighbouring values in the figure is accounted for by the small number of skipping cycles at the movement. In order to extract the numerical values from the data obtained that characterize the periods $a_{\max}$ and $a_{\min}$, a regression curve has been drawn. The along-chain nonlinearity is 4.94%.

Strictly speaking, the right way to estimate scanner nonlinearity would be to analyse the calibration coefficients distributed in the scanning space. Afterwards, by using a calibration database, the atom coordinates of the passed chain are corrected and, as a result, some defects and/or mechanical strains could be revealed in the crystal by a residual chain curvature.

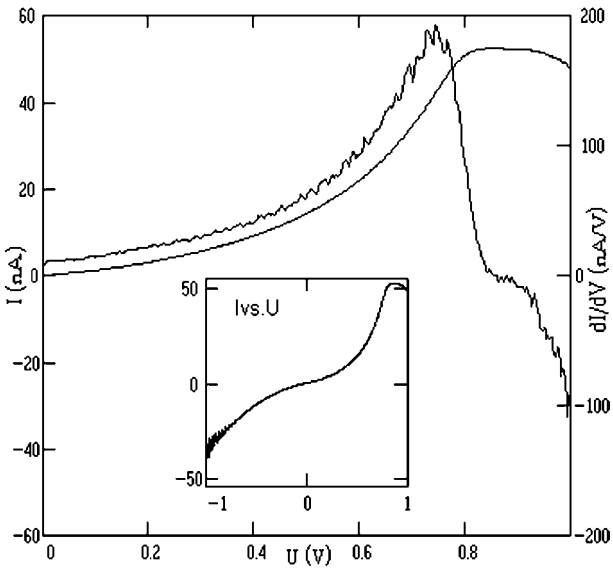

Figure 20. Averaged I–V characteristic of the tunnel junction localized immediately on the apex of the carbon atom. The number of averagings is 10^4. The number of points in one-shot measured curve is 800. The ADC conversion time is 25 μs. The mean modulus of the lateral drift is some 0.29 Å s^{-1}. The measurement time is 57 min. The derivative of the curve is obtained by a three-point symmetrical scheme.

3.5. Accurately localized low-noise spectroscopy

To demonstrate the potential of the method for obtaining spectroscopic information (true spectroscopy data can only be obtained in an ultrahigh vacuum environment), 10^4 measurements of the tunnel junction I versus U curve were carried out. Those measurements interchanged with attachments of the microscope probe to a chosen carbon atom on the graphite surface. An averaged I–V characteristic of

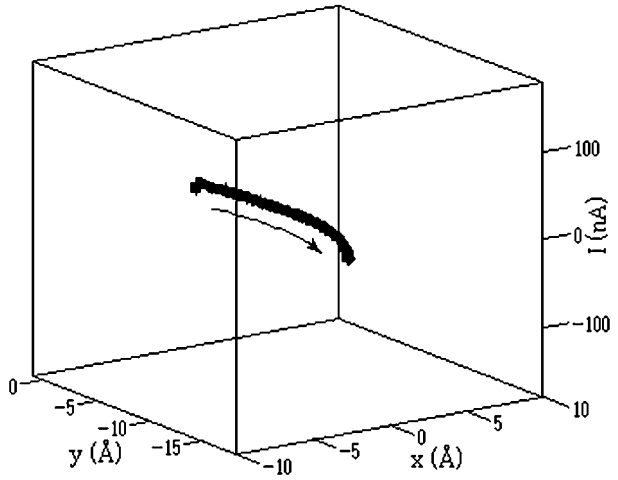

Figure 21. Drift-induced evolution of the attachment atom in space (the arrow designates the movement direction). The mean and maximum drift velocity in the lateral plane are 0.12 and 0.33 Å s^{-1}, respectively. The probable drift direction in the lateral plane is 265°. The '+' sign marks the probe positions. The number of probe attachments is 500. The time interval between the attachments $T = 700$ ms.

the junction and its derivative are shown in figure 20. The I–V characteristic is measured immediately on the apex of the carbon atom (the curve may also be obtained at any point of the atom neighbourhood).

3.6. Determination of microscope drift

Drift measurement consists of sequential probe attachments to a chosen feature on the surface. In figure 21, the spatial trajectory of the attachment atom movement during the measurement is presented. The mean drift velocity of the microscope in the lateral plane equalled some 0.12 Å s^{-1}. One can see in figure 21 that the drift velocity of the microscope appears to be approximately constant over some tens of seconds.

3.7. Feature-oriented scanning of disordered surfaces of electrochemically polished aluminium and plasma-deposited carbon film

The first example illustrating the ability of the algorithm to scan disordered surfaces is a nanostructured aluminium surface presented in figure 22(a). Hereafter the description is made under the following stipulations: the connection method using auxiliary FLs is applied; direct feature recognition is realized; the scanning of apertures and size-fixed segments is carried out with an AFM in tapping mode with fixed step, the spring constant of the NT-MDT cantilever is ∼20 N m^{-1}, the cantilever resonance frequency is 153.403 kHz, and the probe tip radius is less than 10 nm; after assemblage, a mean surface tilt was subtracted from the reconstructed images, and no image smoothing was executed.

As compared with a conventional scan of the same area of the surface (see figure 22(b)), we can see complete reciprocal adequacy of the two images. Creep-induced topography distortions are easily noticeable in figure 22(b), but they are absent in figure 22(a). The structure of the obtained

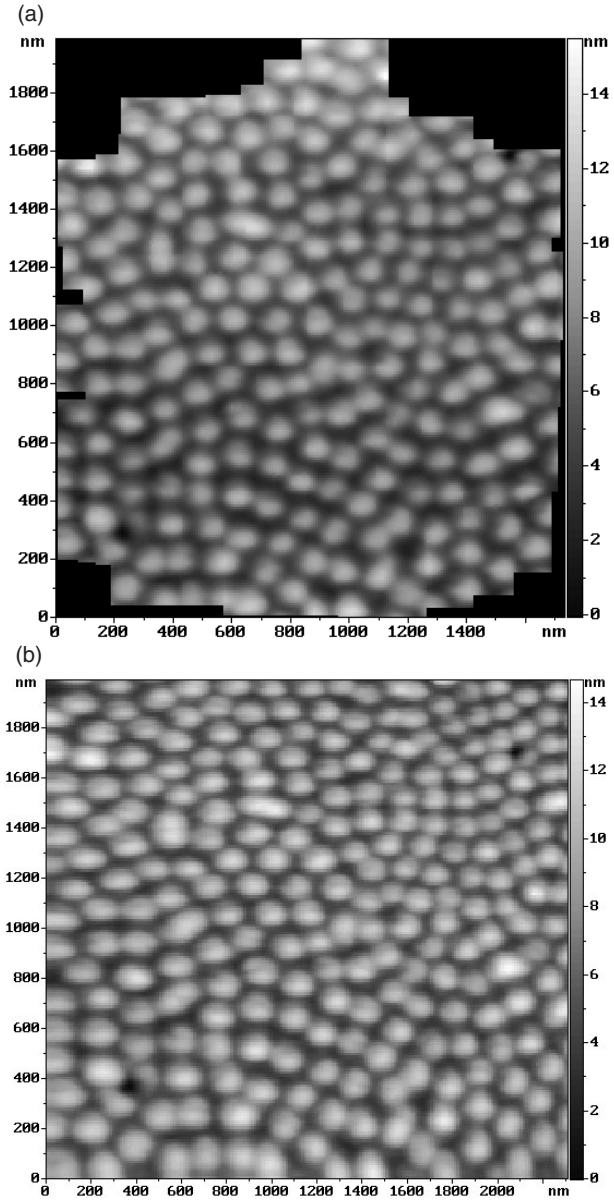

Figure 22. Disordered electrochemically polished aluminium surface (AFM, tapping mode). Steps of the microscope in the lateral plane: $\Delta x = 8.53$ nm, $\Delta y = 8.58$ nm. Image (a) is obtained using FOS. The mean size of the aperture is (59 × 59) $pixels^2$. The segment size is (35 × 35) $pixels^2$. The number of samples in a raster point is 1. The number of skipping cycles is 2. The number of segment averagings is 4. The scanning velocity in the aperture/segment is 3485 nm s^{-1}. The movement speed at skipping is 697 nm s^{-1}. The mean modulus of the lateral drift velocity is some 0.396 Å s^{-1}. The mean modulus of the vertical drift velocity is some 0.077 Å s^{-1}. The scanning time is 8.5 h. Image (b) (198 × 190) $pixels^2$ is obtained by conventional scanning. The statical piezoscanner nonlinearity was corrected by the software. The number of samples in a point is 4. The scanning velocity is 3485 nm s^{-1}. The scanning time is 2 min.

feature chain is shown in figure 23. Some statistics on disordered surface features collected during the measurements are given in table 1. The feature diameter is defined as the diameter of a circle circumscribed over the feature basement. Compactness [10] refers to the percentage of discrepancy in form of the given feature basement as compared to a circle,

Table 1. Statistics (mean values) of features of the disordered surface. The chain length (sample size) is 150 features.

Surface	Type of feature	Distance between features (nm)	Feature basement square (nm^2)	Feature diameter (nm)	Feature height/ depth (nm)	Feature volume (nm^3)	Compactness of feature basement (%)	Density of features (μm^{-2})
Aluminium foil	Hill	132.42	6890.1	93.7	3.46	11 933.7	78.5	51.4
		129.39	7328.1	96.6	4.04	14 595.7	78.3	52.8
Carbon film	Hill and pit	86.82	1821.3	48.2	1.31	1 309.2	71.6	118.7

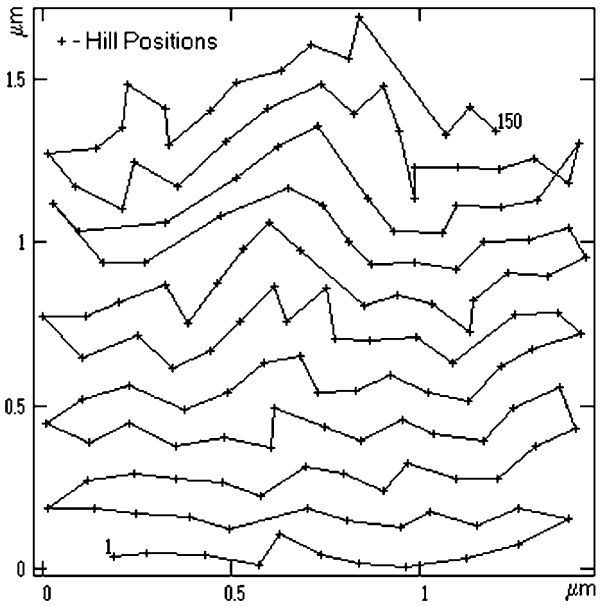

Figure 23. The structure of the feature chain obtained during FOS of the nanostructured aluminium surface.

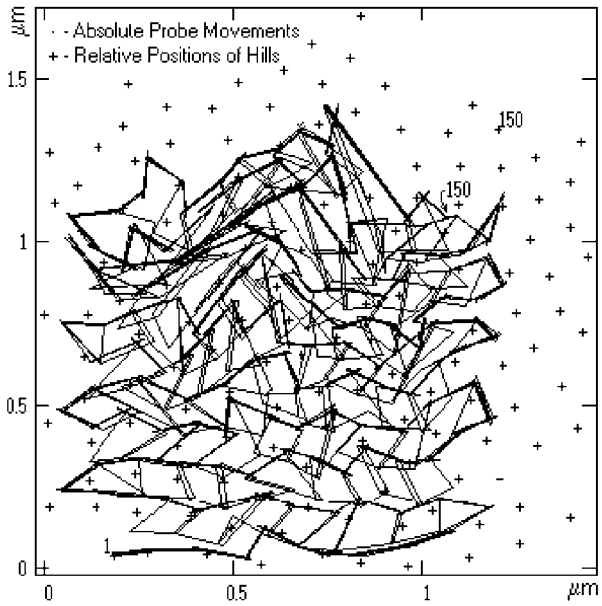

Figure 24. Real net of feature absolute positions overlapped by relative positions. A large difference between absolute and relative positions of the same features points to strong distortions during SPM measurements.

which form is assumed to be of perfect (100%) compactness. If required, distribution histograms can be built for the parameters presented in the table.

During the work, 142 apertures and 600 segments were totally scanned that shows up the high redundancy of the FOS method; also executed were 420 attachments, 364 preskipping cycles (see below), 97 aperture rescans, and 178 segment rescans, which reveals considerable creep-induced motion; the aperture adjustment was carried out 14 times. Figure 24 enables one to clearly estimate the degree of distortions the microscope drift leads to. Here, the absolute and the relative feature coordinates are overlapped by matching positions of the first chain features (compare with figure 11).

Figure 25 shows the same aluminium surface area as in figure 22(a), scanned under the same conditions and with the same parameters, namely, start feature, number of elements per seed, seed orientation, chain length, connection method, number of averagings, initial aperture size, segment size, thresholds, tolerances, etc. The only difference consists in the aperture and segment scan velocity as well as in the skipping movement velocity, which were half the primary value. Directly comparing the topography in figure 25 to that in figure 22(a), reveals a very slight dependence of the reconstructed images upon the scan speed (see also table 1).

To demonstrate evidence of the coincidence of the measured feature coordinates, figure 26 presents the chain corresponding to the topography of figure 25 as well as the feature positions of the topography in figure 22(a) (coincidence of the features is carried out by using least mean squares). The mean mutual deviation is 3.79 nm, which is slightly less than half the scan step used. It should be observed that the small chain mismatch is mostly caused by fluctuations of the microscope settings during a long scan time rather than by drift; another noticeable source of errors is an uncontrollable slight modification of the soft aluminium surface.

Direct comparison of the chains in figures 23 and 26 permits one to reveal small distinctions in their structure, which point out that in the real mode there is no exactly reproducible trajectory of movement from one feature to another. Although the 'macrostate' of the instrument and the 'macroconditions' of the measurements remain practically unchanged, the 'microstate' of the instrument and the 'microconditions' in a particular place of the sample are notably changing, and on scanning the same chain feature are different each time.

One more scan example is given in figure 27, presenting a disordered plasma-deposited carbon film surface. As the substrate, electron resist (methylmethacrylate) was used pre-irradiated with ultra-violet ($\lambda = 180 \cdots 260$ nm) for better flatness. Here, unlike the previous scans, both hills (carbon clusters) and pits (intercluster spaces) were treated as features.

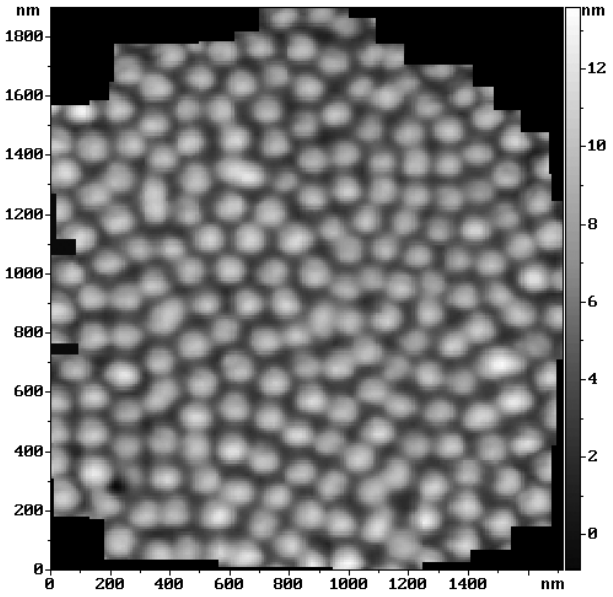

Figure 25. The same aluminium surface area; conditions, modes, and parameters are the same as with topography measuring in figure 22(a) except for the scan velocity, which now is a half-value of the initial velocity in the aperture, in the segment, and at skipping, respectively.

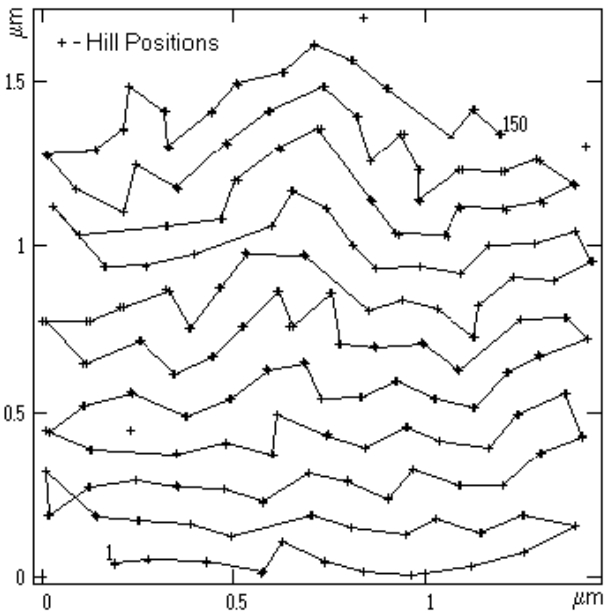

Figure 26. Structure of the feature chain corresponding to the scan in figure 25. The coordinates of the topography features in figure 22(a) are given for reference. The coordinate mean mismatch is 3.79 nm.

The feature chain structure is shown in figure 28. The surface is completely disordered; its characteristics are given in table 1. As compared to the previous surface, a greater dispersion of the feature sizes and distances between the features is noticeable, as well as smaller feature sizes. From figure 29, one can estimate the distortions arising while scanning the carbon film.

In order to restrain the creep while scanning, extra attachments were automatically initiated and preskipping was implemented. Preskipping, or idle skipping, is inserted before

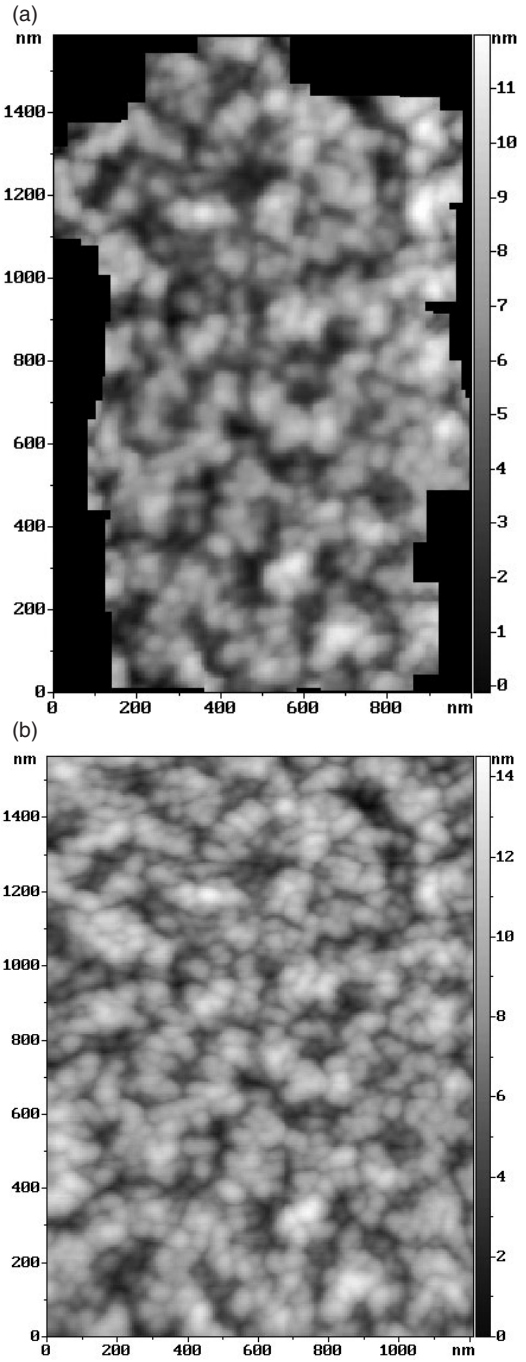

Figure 27. Completely disordered surface of plasma-deposited carbon film (AFM, tapping mode). Steps of the microscope in the lateral plane: $\Delta x = 5.39$ nm, $\Delta y = 5.42$ nm. Image (a) is obtained using FOS. Both hills and pits were used as features (95 and 55, accordingly). The mean size of the aperture is (61×61) pixels^2. The segment size is (41×41) pixels^2. The number of samples in a raster point is 1. The number of skipping cycles is 2. The number of segment averagings is 4. The scanning velocity in the aperture is 1542 nm s^{-1}. The scanning velocity in the segment is 1927 nm s^{-1}. The movement speed at skipping is 385 nm s^{-1}. The mean modulus of the lateral drift velocity is some 0.146 Å s^{-1}. The mean modulus of the vertical drift velocity is some 0.018 Å s^{-1}. The scanning time is 10 h 10 min. Image (b) (180×245) pixels^2 is obtained by conventional scanning. The statical piezoscanner nonlinearity is corrected by the software. The number of samples in a point is 4. The scanning velocity is 1927 nm s^{-1}. The scanning time is 3 min 40 s.

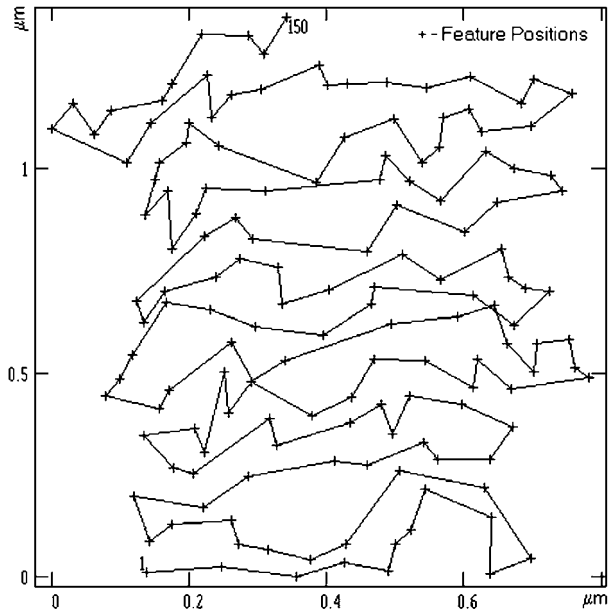

Figure 28. The structure of the feature chain obtained during FOS of the carbon film surface.

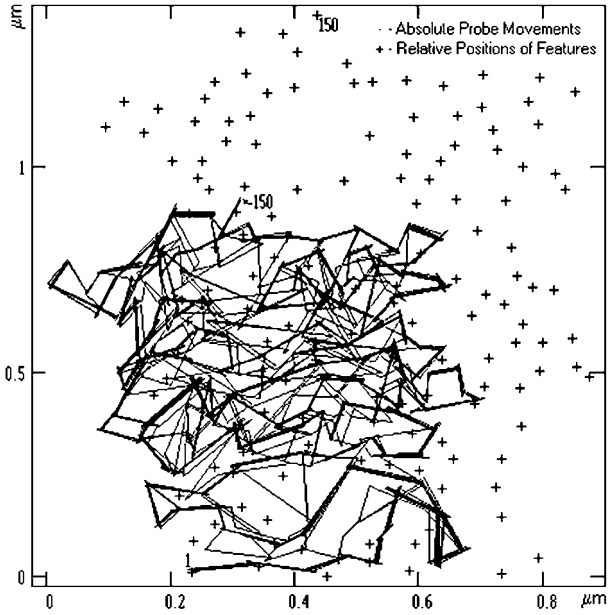

Figure 29. Real net of absolute positions of carbon film features overlapped by relative positions.

the main skipping cycle. Because of large distortions, its results are not used for averaging of the relative distance between features, and only serve as the initial data to launch the main cycle.

Preskipping usually takes 1–3 cycles and provides a smoother transition to the skipping from aperture scanning or from previous skipping. For comparatively large distances between features, at least one preskipping cycle is necessary in order to form a particular hysteresis loop for the main skipping cycle. Such an index as density (see table 1) which is responsible for efficient applicability of the FOS might be quite acceptable when considered for the given surfaces.

In spite of the fact that the sizes of the features, distances between the features, and the scan time of the segment on the presented disordered surfaces are by 2–3 orders greater than the ones on the atomic graphite surface, the measured drift values proved to be comparable, which directly indicates practically complete creep compensation during FOS in size scale up to 100–150 nm.

4. Discussion

Since the method developed implies recognition of the image scanned, the term 'topography features' should be understood in the broad sense. It refers not only to pure topography, but also to physical inhomogeneities such as magnetization domains, places of localized electric charge, and so forth. Therefore, the method described is generally applicable to a wide family of scanning probe devices. For example, it can be used with a magnetic force microscope, electrostatic force microscope, scanning near-field optical microscope, and many others, including the scanning electron microscope.

Initially, the distortion factors were divided into two groups. The first, the timing group, included thermodrift and creep; the second, the spatial one, included nonlinearity, hysteresis, cross coupling, and nonorthogonality. Within each of the groups a further division is neither required nor apparently possible to make in full measure.

Since pinpoint accuracy of measurements with the demonstrated method is achieved at the cost of an abrupt decrease in scanning productivity (a large number of averagings, additional probe movements, high data redundancy), practical use of the algorithm is mostly determined by long-term stability and fast-acting [18] of the microscope. The faster the scanning at the separate atom scale occurs, the slower the process of change in thermal drift looks against its background, and the smaller is the linearization error with the scheme applied.

At present, several systems have been developed with active dynamic correction of microscope piezomanipulators [19–21] which permit accurate measurement of surface topography. The correction is implemented by means of three servosystems (one for each manipulator) embedded into the device control loop. While scanning, a following system tries to compensate for the difference between the set movement value and the actual one which is measured with a linear position sensor.

In spite of good results, closed-loop systems have certain drawbacks. First, they are complex and expensive as they include a reference frame ensuring orthogonality and straightness of the base surfaces with high accuracy as well as three additional control loops each equipped with a high-gain, low-noise position sensor. The reference frame is fabricated of special materials with low thermal expansion coefficient with the use of high precision machining. Frame imperfection leads to cosine error [2].

Second, with those systems there is no way to determine the movement of the probe tip *in situ* since the sensors register manipulator displacement relative to the instrument reference frame. As a result, an Abbé offset error [2] occurs because the manipulator would flex as it works, the sample thickness (probe length) being finite. Third, the above systems are incapable of measuring topography precisely with the ultimate resolution of

the microscope. Fourth, the systems do not allow for holding the microscope probe at a certain surface position during an arbitrarily long time.

Finally, the microscope described in [21] is hardly applicable in those cases when the specific scale of the surface topography being investigated differs significantly from the atomic scale of the standard HOPG surface, because the measurement time may grow unacceptably long for the need of using a small step. Yet another problem is that there are practically no crystal lattices that are defect-free, mechanically relaxed, and evenly ordered along the whole surface. Therefore, the image part having been corrected by an imperfect area of the standard surface will appear distorted.

In contrast, the proposed scanning method appears to be free from the errors and the drawbacks mentioned, requiring no additional mechanical or electronic units. The Abbé offset error is eliminated during the distributed calibration. It is necessary only to provide for a fixed displacement of the scanning plane from the manipulator edge by means of a special sample (tip) holder.

Since the Abbé offset error increases with moving towards the edge of the scanning field, another way to decrease its influence would be to transfer the region being measured from the periphery to the centre of the fine scanner field by means of the coarse positioner and probe-to-feature attachment. To achieve the best results it is recommended to apply the latter method combined with distributed calibration.

In the proposed positioning conception, the cosine error is absent since there is no explicit reference frame. Instead, the XYZ piezoscanner itself partially works as the reference frame only determining the coordinate origin, which coincides with the manipulator position after applying a zero potential on it. Such frame attributes such as axis orthogonality and slideway straightness are implemented by means of distributed calibration. Small thermal deformability of the reference frame, which is usually ensured by the use of special materials and design solutions, is now implemented by active thermal drift compensation during FOS.

It is necessary to note in conclusion that the discussed approaches to surface measurement should not be thought of as opposite to each other; in a number of cases their joint application is expected to yield essentially better results than separate application of either.

Acknowledgments

This work was supported by the Russian Foundation for Basic Research (project nos 96 02 17870, 00 02 17259, and 02 03 32615), by the Fund for Physics of Solid Nanostructures (project no 96 2012), and by Moscow City Government (grant no 1.1.82). The author is grateful to O E Lyapin for checking the manuscript, to Dr S A Gavrilov for the nanostructured aluminium sample provided, to A G Kirilenko for fabrication of the carbon film sample, and to Dr S A Saunin for help in the implementation of the scanning algorithm in a microscope control program.

References

[1] Pohl D W 1986 *IBM J. Res. Dev.* **30** 417
[2] Griffith J E and Grigg D A 1993 *J. Appl. Phys.* **74** R83
[3] Yurov V Y and Klimov A N 1994 *Rev. Sci. Instrum.* **65** 1551
[4] Jørgensen J F, Madsen L L, Garnaes J, Carneiro K and Schaumburg K 1994 *J. Vac. Sci. Technol.* B **12** 1698
[5] Lapshin R V 1995 *Rev. Sci. Instrum.* **66** 4718
[6] Vieira S 1986 *IBM J. Res. Dev.* **30** 553
[7] Stoll E P 1992 *Ultramicroscopy* **42–44** 1585
[8] Lapshin R V 1999 *Russian Patent Specification* 2 175 761 (available at www.nanoworld.org/homepages/lapshin/patents.htm)
[9] Lapshin R V 2002 *PhD Thesis* Moscow (in Russian, available at www.nanoworld.org/homepages/lapshin/publications.htm)
[10] Lapshin R V 1998 *Rev. Sci. Instrum.* **69** 3268
[11] Pohl D W and Möller R 1988 *Rev. Sci. Instrum.* **59** 840
[12] Swartzentruber B S 1996 *Phys. Rev. Lett.* **76** 459
[13] Lapshin R V 2004 *Russian Patent Specification* (under registration)
[14] Yuzhakov V V, Chang H C and Miller A E 1997 *Phys. Rev.* B **56** 12608
[15] Lapshin R V 1999 *Russian Patent Specification* 2 181 212
[16] Binnig G and Rohrer H 1983 *Surf. Sci.* **126** 236
[17] Lapshin R V 2000 *Rev. Sci. Instrum.* **71** 4607
[18] Lapshin R V and Obyedkov O V 1993 *Rev. Sci. Instrum.* **64** 2883
[19] Griffith J E, Miller G L, Green C A, Grigg D A and Russell P E 1990 *J. Vac. Sci. Technol.* B **8** 2023
[20] Barrett R C and Quate C F 1991 *Rev. Sci. Instrum.* **62** 1393
[21] Kawakatsu H, Hoshi Y, Higuchi T and Kitano H 1991 *J. Vac. Sci. Technol.* B **9** 651